Analysis of capillary-like structures formed by endothelial cells in a novel organotypic assay developed from heart tissue

Simon Bowyer [1]

simonbowyer@gmail.com

Chryso Kanthou [2]

c.kanthou@sheffield.ac.uk

C. C. Reyes-Aldasoro [3]

reyes@city.ac.uk
http://staff.city.ac.uk/~sbbk034/

[1] University of Sussex, Brighton UK

[2] Tumour Microcirculation Group,
The University of Sheffield,
Sheffield, UK

[3] Biomedical Engineering Research
Group, City University London,
London UK

Abstract

In this work, we present an algorithm to perform automatic segmentation, feature extraction and dosage classification of images derived from a novel organotypic angiogenesis assay developed to assess the effects of ionising radiation in the mouse heart. The images presented very different conditions of illumination and conditions of density and shapes of cells. The algorithm consists of a pipeline of several steps, which were validated against hand-segmented images. The algorithm provided satisfactory results, as all images were correctly dose-classified. The cells exposed to the lowest radiation dose were observed to have the greatest relative feature variability.

1 Introduction

Formation of new blood vessels by angiogenesis is a feature of embryonic development, while in the adult, angiogenesis is associated with several pathological conditions such as cancer, as well as normal physiological tissue repair processes. For example, in the heart, injury triggers repair mechanisms within the myocardium, which are dependent on angiogenesis. For example, following a myocardial infarction, ischaemia triggers vascular responses and new blood vessel formation/angiogenesis aiming to repair the damage and re-establish flow [1]. Various organotypic assays have been developed in order to model the angiogenic process, test therapeutic agents and analyse the molecular mechanisms involved [2]. In these assays, which are generally based on co-culturing endothelial cells with fibroblasts, the endothelial cells migrate and align to form capillary-like structures embedded within fibroblasts and matrix. We have recently developed a heart angiogenesis organotypic assay by culturing enzymatically digested heart tissue fragments [3]. In this

model, cardiac endothelial cells form tubule-like structures embedded within the various cellular components of the digested heart tissue, which include fibroblasts and pericytes. We used this model system to establish the effects of ionising radiation on heart microvascular damage and inhibition of angiogenesis. This paper is concerned with the geometric analysis of these tube-like structures using cultures derived from the hearts of C67BL/6 mice that were irradiated with a range of ionizing radiation doses (0.2, 2, 8, 16 Gy) [n=4x4] and sham-irradiated controls [n=4]. The hearts were excised for assay at 20 weeks post irradiation. One of the 8 Gy images was discarded due to duplication, leaving 19 images in total.

2 Materials and Methods

Organotypic cultures were stained with lectin to identify the endothelial cells and a representative image at each irradiation dose is shown in Fig. 1. The images are greyscale, with low contrast, each 696x520 pixels in size and comprising a cluttered background overlaid with the tube-like structures formed by endothelial cells (white arrow). There are significant inter-image and intra-image shading variations. Dead cells or debris were also present, sometimes occluding the tubules (black arrow). The tubules were the primary target of the analysis, though the debris (biological in nature rather than imaging artefacts) is also relevant.
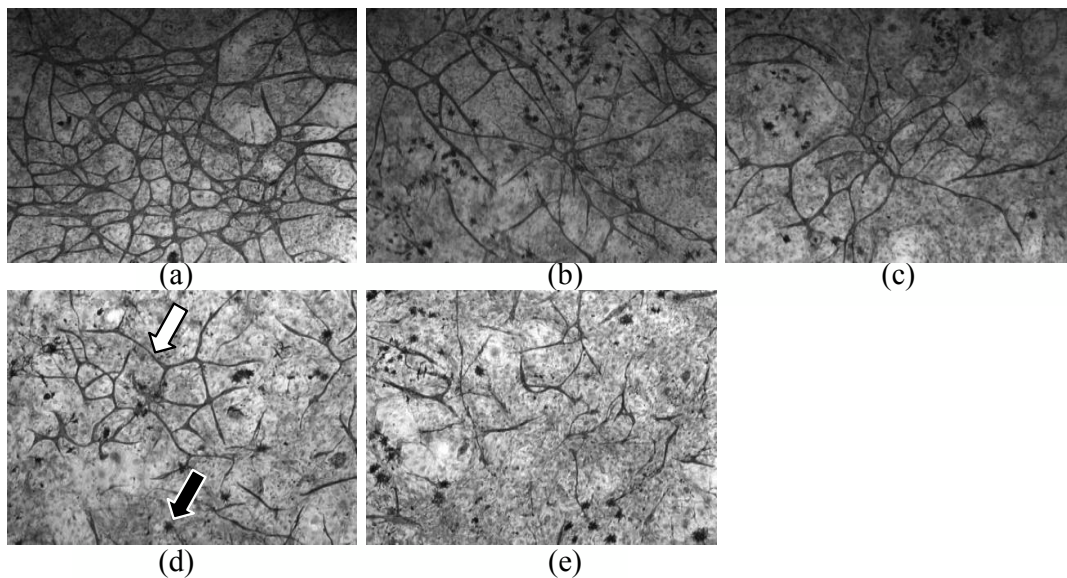

Figure 1: Representative images of the image set; white arrow marks tubule, black arrow marks debris. Irradiation doses: (a) 0 Gy, (b) 0.2 Gy, (c) 2 Gy, (d) 8 Gy, (e) 16 Gy.

The automatic segmentation was validated against manual segmentation (Fig. 2), performed within the MATLAB *roipoly* function by one of the authors without knowledge of the subsequent algorithm or of the automatic segmentation results.
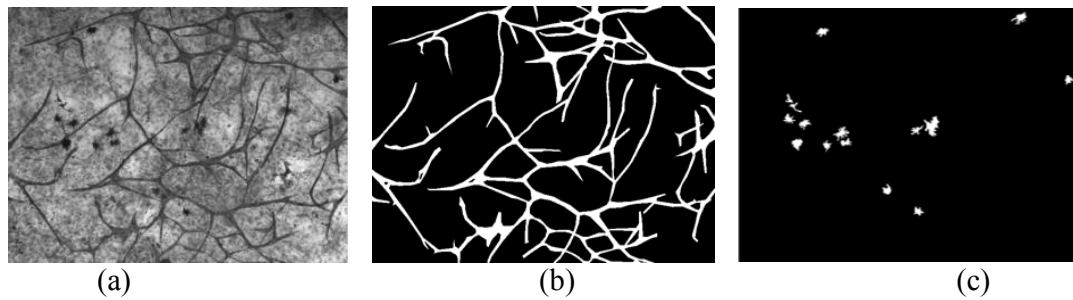
| (a) | (b) | (c) |

Figure 2: Manual segmentation (a) original image, (b) tubules, (c) debris.

An automatic segmentation script was developed in MATLAB with the following steps: 1) Median filtering with a 5×5 pixel neighbourhood using *medfilt2*(); 2) Thresholding based on the local mean of each 151×151 neighbourhood, for each pixel > $0.75\,\bar{x}$ and $> 1\,\sigma$ [4, p. 527]; 3) Removal of noise, i.e. objects with area < 25 pixels; and 4) Removal of likely debris, i.e. objects of solidity > 0.6. 'Solidity' is the proportion of the number of pixels in an object's convex hull which are also in that object [5]. This step removes objects that are insufficiently spindly to be tubules. These steps are illustrated in Table 1.

MATLAB function	Implementation	Output (close view)
	Original image	
medfilt2()	De-noise while retaining edges by applying a median filter with a 5x5 pixel neighbourhood	
localthresh()	Threshold using local means with 151x151 neighbourhood, std dev multiplier of 1, mean multiplier of 0.75. These parameters produced peak mean segmentation correlation for all images.	
bwarea()	De-speckle by deleting all binary objects of area < 25 pixels	
regionprops()	Remove debris, i.e. binary objects with solidity > 0.6 (pixels in object / pixels in convex hull)	

Table 1: Automatic segmentation algorithm pipeline

The following feature metrics were extracted from the segmented images: 1) Relative tubule area, as a proportion of total image area; 2) Euler number (i.e. number of 'holes' in the tubule mesh) as a proxy for the count of regions completely enclosed by tubules (*bweuler*); 3) Largest major axis of the tubule objects in the image, as a proportion of the diagonal image size; and 4) Largest minor axis of the tubule objects in the image, as a proportion of the diagonal image size. These features were selected for their discrimination properties. No formal means of feature selection was used; we leave that as further work.

The extracted features were classified with the function *treebagger* [6][7], to grow regression and classification decision trees with the intent of automatically placing the target images into dosage categories. The same function was also reapplied with the intent of automatically estimating the dosage exposure as a continuous value.

3 Results

Validation was performed as a binary pixels-by-pixel comparison against the manual ground truth (Fig. 3). The results of the classification algorithm showed a mean misclassification for all target images of 0.0733 ±0.0455. Misclassification overall ranged between 0.0263 and 0.2059. The visible output of the automated segmentation method when applied to two sample images is shown in Fig. 4.
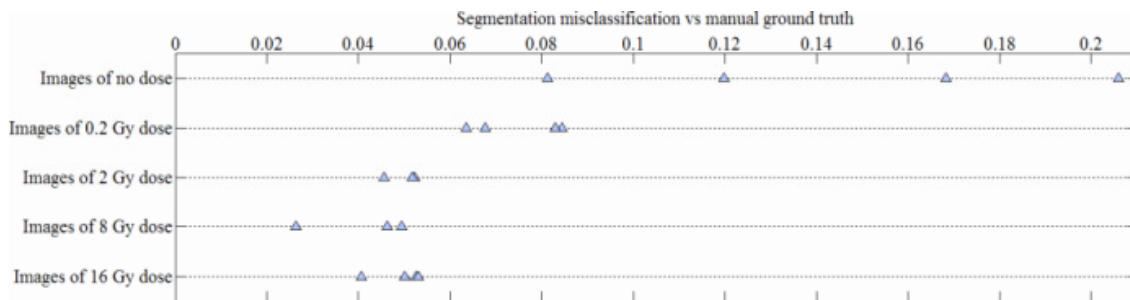

Figure 3: Automatic segmentation accuracy against manual ground truth, grouped by dose. Performance on irradiated images is considerably better than on control images.

Comparison of two of the extracted feature metrics is presented in Fig. 5a (manual segmentation) and Fig. 5b (automatic segmentation). From inspecting Fig. 5a, it is apparent that the largest relative biological morphological variation is present in a healthy specimen exposed to the smallest dose of radiation (0.2 Gy). Even with only two feature dimensions plotted, the topological changes between 0 and 0.2 Gy are greater than those changes that occur between 0.2 and 2 Gy.

The grouping of vector sets into obvious clusters indicates suitability for the application of automatic classification techniques, though 8 Gy and 16 Gy images are difficult to separate when only these two features are examined. It can be seen that the cluster separation is reasonably clear in the data extracted from the manually segmented images (Fig. 5a), and that the clusters are noticeably less separated in the data extracted from the automatically segmented images (Fig. 5b). This indicates that there is low-dimensional information loss in the automatically segmented images due to segmentation inaccuracy.

All automatically segmented images were correctly dose-classified (Table II). The dose-classification confusion matrix of the *treebagger* was extremely good; this is thought to be

due to the dose-discrimination exhibited by the extracted features. Though *treebagger* (being a random forest algorithm) assigns ⅔ of inputs to training and ⅓ to testing and so cross-validation is not required, there were few images and no measurement of misclassification cost was attempted. The feature extraction appeared to be robust to the misclassifications of the segmentation process. Mean classification confidence is 0.83 ± 0.11. Minimum classification confidence is 0.66, for one image of 2 Gy dosage.
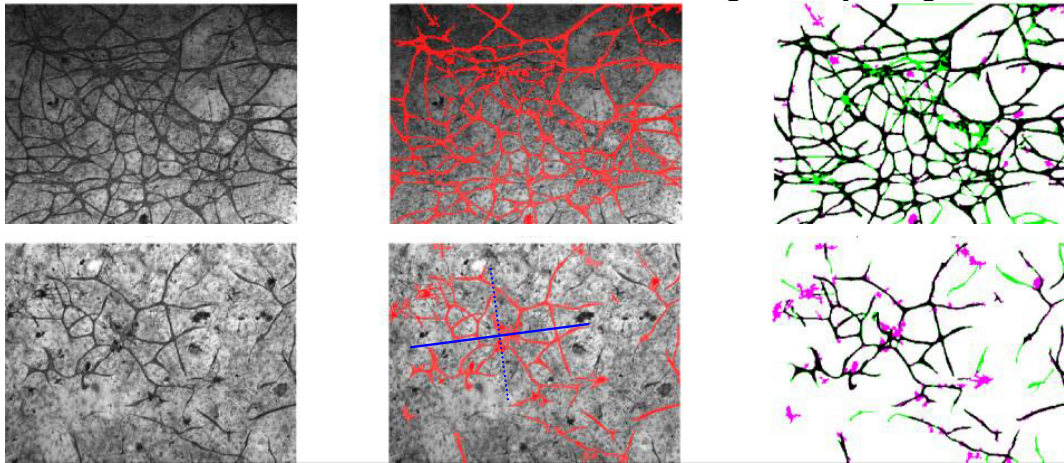

Figure 4: Segmentation results: (left) representative images; (centre) automatically-segmented tubules overlaid in red; (right), validation: correct segmentation (black) false positives (magenta), false negatives (green). Largest second-moment major and minor axis region features are plotted as solid and dotted blue respectively (centre lower), these features are thought to assist with measurement of tubule fragmentation. A dark image seems to have missed tubules, whilst a bright image segmented background and debris as tubules.
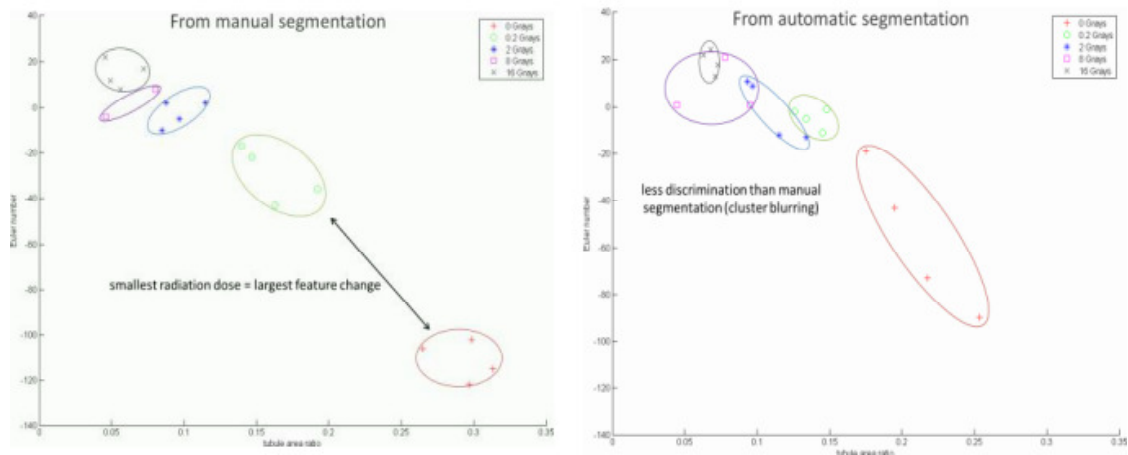

Figure 5: (a) Plot of Euler number vs. tubule area ratio extracted from manual segmentations. There is an inverse relationship between tubule area ratio and Euler number. Note the cluster discrimination, and that the largest feature change is caused by the smallest radiation dose. (b) Plot of Euler number vs. tubule area ratio extracted from automatic segmentations. Note the reduced cluster discrimination in comparison to the manual segmentation in Fig 5(a).

Images at dose, Gy	Classification category				
	'0'	'0.2'	'2'	'8'	'16'
0	**0.88**	0.08	0.04	0.02	
0.2	0.05	**0.78**	0.14	0.06	
2	0.07	0.11	**0.76**	0.21	0.02
8	0.01	0.05	0.15	**0.77**	0.12
16			0.02	0.04	**0.96**

Table 2: Dose-classification mean confusion matrix derived from automatic segmentation

4 Conclusion

Automated segmentation of the source images was mildly successful, with an automated algorithm pipeline giving pixel-level misclassification versus manually segmented images of minimum 0.026, mean 0.073, and maximum 0.206. Four spatial features with high dosage discrimination were identified and then applied to reduce the segmented images to low-dimensional form. The smallest radiation dosages cause the largest relative cell structure feature changes. This is clearest when extracting features based on manual segmentation, though is still apparent when using automated segmentation. All images were correctly automatically dose-classified with > 65% confidence and five images with > 95% confidence. This indicates that an automatic segmentation and classification algorithm can be applied to classify and investigate the characteristics of the effects of radiation on cardiac tissue. We plan to extend the algorithm, investigating the effect of the shading [8] on the segmentation and classification, we will consider other classifiers and test it with a larger database in the future.

References

[1]   R. Khurana, M. Simons, J. F. Martin, and I. C. Zachary, "Role of angiogenesis in cardiovascular disease: a critical appraisal," *Circulation*, vol. 112, no. 12, pp. 1813–1824, Sep. 2005.

[2]   C. Hetheridge, G. Mavria, and H. Mellor, "Uses of the in vitro endothelial-fibroblast organotypic co-culture assay in angiogenesis research," *Biochem. Soc. Trans.*, vol. 39, no. 6, pp. 1597–1600, Dec. 2011.

[3]   C. Kanthou, Z. Gharaei, J. Haagen, S. J. Lunt, C. C. Reyes-Aldasoro, W. Doerr, and G. M. Tozer, "Abstract 5723: Inhibition of angiogenesis in the mouse heart by ionizing radiation," *Cancer Res.*, vol. 72, no. 8 Supplement, pp. 5723–5723, Apr. 2012.

[4]   R. C. Gonzalez, S. L. Eddins, and R. E. (Richard E. Woods, *Digital image processing using MATLAB*, 2nd ed. [U.S.]: Gatesmark, 2009.

[5]   "regionprops: Measure properties of image regions," *MATLAB R2013a online documentation*. [Online]. Available: http://www.mathworks.co.uk/help/images/ref/regionprops.html. [Accessed: 18-Aug-2013].

[6]   L. Breiman, "Random Forests," *Mach. Learn.*, vol. 45, no. 1, pp. 5–32, Oct. 2001.

[7]   "Ensemble Methods - Bag," *MATLAB R2013a online documentation*. [Online]. Available: http://www.mathworks.co.uk/help/stats/ensemble-methods.html#bsw8at7. [Accessed: 18-Aug-2013].

[8]   C. C. Reyes-Aldasoro, "Retrospective shading correction algorithm based on signal envelope estimation," *Electron. Lett.*, vol. 45, no. 9, p. 454, 2009.